Accepted Manuscript

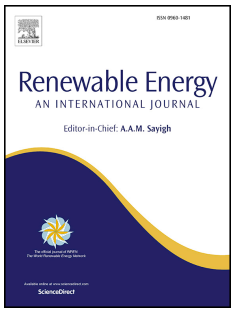

An experiment of a hydropower conversion system based on vortex-induced vibrations in a confined channel

Nicolas Dellinger, Pierre François, David Lefebure, Robert Mose, Pierre-Andre Garambois

PII: S0960-1481(17)30751-6

DOI: 10.1016/j.renene.2017.07.122

Reference: RENE 9097

To appear in: *Renewable Energy*

Received Date: 28 August 2016

Revised Date: 22 May 2017

Accepted Date: 30 July 2017

Please cite this article as: Dellinger N, François P, Lefebure D, Mose R, Garambois P-A, An experiment of a hydropower conversion system based on vortex-induced vibrations in a confined channel, *Renewable Energy* (2017), doi: 10.1016/j.renene.2017.07.122.

An experiment of a hydropower conversion system based on vortex-induced vibrations in a confined channel

Nicolas Dellinger, Pierre François, David Lefebure, Robert Mose, Pierre-Andre Garambois

Laboratoire des sciences de l'ingénieur, de l'informatique et de l'imagerie (ICUBE), Strasbourg, France

Abstract

A hydropower conversion system based on vortex-induced vibrations is investigated experimentally. It consists in a cylinder immerged in a low-velocity flow in a channel (under 1 m/s), wich is linked to a variable stiffness spring, so that the natural frequency of the system might be controlled. Current studies report investigations on marine applications. Although rivers or channels constitute a strong energy potential, they are not exploited enough. In this paper, we will investigate the feasiblity of such a system implantation in a confined flow in a channel, with important edge effects. We propose a study of the effects of a confined flow on the efficiency of the system. We will highlight feasible improvements, particularly through automatic control strategies (generator behaviour, system's natural frequency). Moreover, we show the strong influence of confinement on the flow topology through velocity field measurements using *pulse-pair* method.

Keywords: vortex-induced vibrations, hydraulics of renewable energy systems, non-linear resonant, velocity, measurements, vortex dynamics.

1. Introduction

Promoting the development of new, safe and renewable energy sources has become more than a priority. Over the last ten years, great advances have been made in developping fluid-flow kinetic energy conversion systems. In most cases, these systems are intended for marine applications, operating in currents higher than 2 m s^{-1} whereas low current sites are under or even unexploited. This ressource represents an amount of 1 GW according to Bal and Chabot (2001), concerning upstream river reaches, low head dams, unexploited mills or even irrigation channels. As a matter of fact, all those hydropower ressources involve confined flows with significant boundary effects that have to be accounted for optimizing hydropower conversion.

Systems based on vortex-induced vibrations (VIV) are an efficient way to recover kinetic energy from low currents. Few prototypes or models are currently developed. Grouthier et al. (2014) propose a numerical model, which is able to estimate the amount of harvested energy using VIV on cables. Singh et al. (2012) propose a theoretical model of a wake oscillator based on VIV. They determine an optimized mechanical configuration and orientation of the structure in the flow in order to improve its efficiency. Another prototype based on this phenomenon using a rigid cylinder is developed by Bernitsas et al. (2008), in the VIVACE framework. The authors explore the possibility of energy harvesting in low currents in semi infinite domains.

In this system, vortices are formed and shed on the downstream side of a cylinder. Vortex shedding alternates from one side of the cylinder to the other, thereby creating a pressure imbalance resulting in an oscillatory lift. Then, the mechanical energy of VIV has to be converted. In its simplest form, a converter modulus consists in mass-spring-damper system with one degree of freedom crossflow. With such a device Bernitsas et al. (2008) demonstrate that energy can be harvested from flow velocities as low as 0.25 m s^{-1}. The behaviour of VIV of a cylinder for various flow conditions are studied experimentally by Zdravkovich (1997). This study deals in particular, with vortex shedding modes and frequencies for a large range of Reynolds numbers. A strong dependency of the oscillation amplitude on Reynolds number is highlighted. An optimal range of Reynolds number between 10^4 and 10^5 is identified for energy harvesting by Raghavan and Bernitsas (2011).

Optimizing VIV based hydropower systems is necessary and relies on complementary improvements given the complexity of the fluid-structure interactions. Lee et al. (2011) propose to use an automatically controlled motor/generator instead of damper and spring systems, which allows to cover a wide range of damping effects, hence flow conditions plus mechanical systems configurations. With

such a device, Lee and Bernitsas (2011) demonstrate the ability of the VIVACE converter to extract energy with large aspect ratio (ratio between the cylinder length and its diameter) and blockage ratio (ratio between the occupied surface of the cylinder and the upstream section), far away from the water surface. They present oscillation frequency and amplitude as a function of the stiffness and of the linear damping parameter.

Concerning the VIVACE converter, two main ways of improvement are proposed in the literature . The first deals with the developement of a feedback control strategy based on flow measurement. The elaboration of a closed loop control strategy for low Reynolds number values, gained from asymptotic developments, is proposed by Meliga et al. (2011). Chang et al. (2011), Kiu et al. (2011), Ding et al. (2013) are following another way, focused on the passive control of turbulency. The effects of the surface roughness on the device efficiency are studied both experimentally and numerically. A very strong but complex coupling between turbulence and system behaviour is highlighted with still unclear characterization of the effects of turbulence control. However, the trade-off between harvesting energy induced by oscillations without breaking them is a key issue for VIV systems.

Designing efficient VIV converters for real river sites may involve small aspect ratio of the immersed body, large blockage ratio and confined flow with boundary effects. The present contribution therefore proposes a new experimental characterization of an inovative VIV system composed of a low aspect ratio cylinder and a controllable mechanical system. It is tested in real flow conditions and a new nonlinear law for describing the mechanical action of interest is proposed, that is to say the force induced by the generator on the cylinder. The power coefficient (efficiency), normalized oscillation amplitudes and frequency are presented. An original control strategy of the efficiency based on cylinder velocity feedback is presented. Flow structures variabilities downstream of the cylinder are studied thanks to an original method using ultrasonor transducers and pulse-pair method. This paper is organized as follows: section 2 presents the physical background for VIV; the experimental setup and measurement with a specific velocity profiler are described in section 3. Results and discussions are presented in section 4 before concluding in section 5.

2. Background

If a rigid cylinder mounted on spring is immersed in the flow, forced vibrations can be observed. This fluid-structure interaction phenomenon occurs because of nonlinear resonance of the cylinder through vortex shedding lock-in (responsible of VIV). Note that oscillations of higher amplitude appear in the crossflow plane. The system presented here has a degree of freedom in the vertical direction of the crossflow plane. As stated above, VIV require a trade-off between energy harvesting and flow osscillations. Therefore, this section presents several dimensionless numbers and coefficients of interest.

For a classical Von-Karman vortex street and for a cylinder at rest, the vortex shedding frequency f_v equals the Strouhal frequency f_s. f_s appears in the expression of the Strouhal number describing oscillating flow mechanisms:

$$\mathrm{St} = \frac{f_s D}{u} \qquad (1)$$

where St is the Strouhal number, u is the fluid velocity and D is the diameter of the cylinder. It is assumed that for a Reynolds number R of the order of 10^5 and for a cylinder with an important lenght, $St = 0.2$. When VIV occur, it is assumed that the main frequency of cylinder oscillation in water $f_{c,e}$ is equal to the vortex formation frequency f_v: this case is also called ”lock-in” or synchronisation. Note that some authors (Chang et al. (2011); Raghavan and Bernitsas (2011)) reported wake patterns that do not correspond to a classical Karman vortex street. They define wake-mode terminology to describe the different wake-modes. Therefore, the frequency of the periodic wake vortex mode $f_{v,m}$ is introduced. Thus the synchronisation, or lock-in, is defined as follows:

$$f_{c,e} = f_{v,m} \qquad (2)$$

At synchronisation f_v or $f_{v,m}$ are clearly distinct of f_s. The synchronisation depends on R, on the mass ratio m^* presented below and on the body's natural frequency in water $f_{o,e}$ (influenced by the added mass). This latest frequency is given by the equation:

$$f_{o,e} = \frac{1}{2\pi}\sqrt{\frac{k_{eq}}{m_{eq}+m_a}} \qquad (3)$$

where k_{eq} is the equivalent stiffness, m_{eq} is the equivalent mass in vertical translation, $m_a = C_a \rho_f V_{cyl}$ the added mass, $\mathrm{C_a}$ is the added mass coefficient and V_{cyl} is the volume of the immerged cylinder.

Concerning the C_a coefficient, it is highly depending on the amplitude of oscillations, as shown by Rajaona et al. (2003) experiments, and on values ranging between 0.5 to 2 for a smooth cylinder. In this work a constant value is used according to Gaurier et al. (2003) . Considering that Reynolds number remains constant (5.5×10^4) and that the Keulagan-Carpenter number ($KC = \pi\frac{A}{D}$) is close to 3, it is assumed that C_a remains constant and equal to 2 for all experiments presented hereafter.

The mass ratio m^* is given (Blevins (2001)) by the equation:

$$\mathrm{m}^* = \frac{m_{eq}}{m_a} \qquad (4)$$

According to Bernitsas et al. (2008), when synchronisation occurs for high m^* values, the ratio $f_{c,e}/f_{o,e}$ remains close to 1. For low m^* values, higher distinct values are observed for $f_{c,e}/f_{o,e}$.

3. Experimental setup

As previously mentioned, the synchronisation between cylinder oscilations and vortex shedding depends on body natural frequency $f_{o,e}$, the added mass m^* and the Reynolds number R. While R depends on the flow and the cylinder diameter, $f_{o,e}$ depends on the equivalent spring stiffness and mass. This section details the features of the experimental device.

3.1. The technical architecture

The experimental prototype is tested in free-surface flows in the channel of ICube laboratory. The upstream velocities range from 0.5 to 1 m s^{-1} (cf. Fig. 2). Consequently the diameter of the sealed hollow cylinder, immersed in the flow, is determined to obtain an R between 0.5×10^4 and 1.0×10^5. The spring-supported cylinder has a translational degree of freedom transverse to the flow direction ($\boldsymbol{z}_1$ direction). A spring (*a*) with a constant stiffness k_1 and another one (*b*) with a variable stiffness k_v are used. This association between k_1 and k_v results in an equivalent stiffness k_{eq}, which directly impacts the frequency of body oscillations in water $f_{o,e}$.

The translational mechanical energy is then converted by an electric generator G (*c*), which is driven by a power transmission belt system (*d*). The torque or speed of the generator is controlled by the servo controller. A corrective PID action is used to ensure the system is stable . The incremental encoder T_a is used to measure generator rotor position (θ_g) and speed (Ω_g). The acceleration Γ is measured by an accelerometer (Acc). We use a computer coupled with a data acquisition device for

data acquisition and generator control. The block formed by the PID, the computer and the data acquisition device is called *control system* (*e*).

Figure 1: A basic diagram of the instrumentation, the control system and the mechanical part of the hydropower conversion system.

Figure 2: The hydropower conversion system mounted on the ICube channel.

Table 1: System and channel main features.

Parameters	Values	Experimental conditions
D	0.11 m	0.11 m
L	0.5 m	0.5 m
k_{eq}	400 - 3000 N m^{-1}	830 N m^{-1}
Blockage ratio[a]	-	30 %
m^*	1.22 - 2	1.22 and 1.68
m_{eq}	5.8 - 9.5 kg	5.8 and 8 kg
Mean flow rate Q_v	0 - 700 m^3 h^{-1}	350 m^3 h^{-1}
Mean flow velocity v	0 - 1 m s^{-1}	0.52 m s^{-1}
Channel width	0.6 m	0.6 m

In order to estimate the energy losses in the mechanical part of the system, a classical linear model is used. A damping coefficient C_{system} is introduced. The resulting breaking force F_b on the translation direction $\mathbf{z}_1$ is simply given by the equation:

$$F_b = -C_{system} v_c = -C_{system} \frac{\mathrm{d}z}{\mathrm{d}t} \quad (5)$$

where v_c is the projection of the cylinder velocity on $\mathbf{z}_1$, z is the cylinder position. By applying the fundamental principle of dynamics to the mass-spring-damping system in the air (cf. Fig. 2), we get:

$$m_{eq} \frac{\mathrm{d}^2 z}{\mathrm{d}t^2} + C_{system} \frac{\mathrm{d}z}{\mathrm{d}t} + k_{eq} z = F \quad (6)$$

where F is an external action applied to the cylinder. The position of the cylinder at rest corresponds to $z = 0$. Then the transfer function expression of cylinder displacement $z(t)$ in function of the external force $F(t)$ is derived. The Laplace transform method is used, defined for a causal $g(t)$ integrable function by:

$$G(p) = \mathcal{L}(g(t)) = \int_{0^-}^{+\infty} g(t) e^{-pt} \mathrm{d}t \quad (7)$$

We obtain the following ratio between $z(t)$ and $F(t)$ through their transformed form $Z(p)$ and $\mathcal{F}(p)$:

$$\frac{Z(p)}{\mathcal{F}(p)} = \frac{\frac{1}{k_{eq}}}{1 + \frac{C_{system}}{k_{eq}} p + \frac{m_{eq}}{k_{eq}} p^2} \qquad (8)$$

with $\mathcal{F}(p) = \mathcal{L}(F(t))$ and $Z(p) = \mathcal{L}(z(t))$. This is a second order transfer function and by identification we get:

$$\begin{cases} \frac{1}{\omega_0^2} = \frac{m_{eq}}{k_{eq}} \\ \frac{2\xi}{\omega_0} = \frac{C_{system}}{k_{eq}} \end{cases} \qquad (9)$$

where ω_0 is the natural pulsation and ξ is the dimensionless damping parameter of the mass-spring-damping system.

$$\xi = \frac{C_{system}}{2k_{eq}} \sqrt{\frac{k_{eq}}{m_{eq}}} \qquad (10)$$

An experimental free decay test in the air has been used to identify C_{system}, by measuring $d_{1\%}$, which is the first excedance above the asymptotic value corresponding to static position. It is defined in percentage of exceedance labeled and expressed as:

$$d_{1\%} = 100 e^{-\frac{\pi\xi}{\sqrt{1-\xi^2}}} \qquad (11)$$

Thereby for each value of the cylinder vertical velocity v_c, the breaking force F_b is balanced by the generator thanks to the feedback loop of the control system.

Different control strategies have been developed to optimize energy recovery, as it is described in part 4. The control acts on the generator torque (C_g) based on generator intensity (I_g) and generator velocity (Ω_g) output measurements.

3.2. Velocity measurement technique

While maximum efficiency remains below $\eta = 20\%$ with an optimized control system, the flow behaviour needs to be understood in order to improve the cylinder shape factor and to prevent potential boundary effects. Vortex shedding frequency and mean velocity profiles behind the cylinder are measured, first at rest, then with a vertical degree of freedom. Those experiments are done in order to compare the experimental and theoretical vortex shedding frequencies and investigate the potential presence of sub-harmonics. Moreover, thanks to the accuracy of the velocity measurement technique the boundary effects are quantifiable.

Velocity field measurements are performed with an ultrasonic profiler based on *pulse pair* technique using a combination of two ultra-sonic transducers (Pallares et al. (2011)) (cf. Fig. 4). This device developed at ICube laboratory can record velocity vectors along its beam, namely velocity magnitude, sense and direction. The two transducers are used successively, the first one (T_1) emitting a vertical ultrasonic beam and the second one (T_2) is inclined at an angle $\theta = 15^\circ$ from the vertical in

mainstream direction. Each transducer measures the velocity component in its beam direction, respectively u_{T_1} and u_{T_2} as shown on Fig. 4.

Figure 3: Crossflow view of the cylinder (black rectangle) with its extremal positions (dashed lines rectangles). Notations for surface oscillations amplitude calculation.

Figure 4: Vertical plane view of pulse pair technique device, T_1 and T_2 being the two transducers, downstream of the cylinder (black circle).

At this stage of the study the two components of velocity are not measured exactly at the same location and the same time. That is why instantaneous horizontal velocity *u* cannot thus be obtained. Nevertheless, time averaged horizontal component of velocity $\overline{u}$, can be obtained in case of zero average vertical velocity, $\overline{v}$, or negligible horizontal gradient of vertical velocity. In this case, $\overline{u}$ is computed by solving:

$$\begin{cases} \overline{u_{\tau_1}} & = \overline{v} \\ \overline{u_{\tau_2}} & = \overline{u}\sin\theta + \overline{v}\cos\theta \end{cases} \qquad (12)$$

The whole device can be placed at any desired location in mainstream direction ($\boldsymbol{x}_1$), or lateral direction ($\boldsymbol{y}_1$). In the present paper, transducers are always placed at a distance x_T = 31 cm downstream of the cylinder axis. This device enables a fairly good measurement spatial resolution of 8 mm (resp. 4 mm) at a rate of 12 Hz (resp. 8 Hz) with a maximum relative uncertainty of 3 % . This latter value was calculated for an angle θ which remains constant and equal to 15°, with an uncertainty of $\pm\ 1^{\circ}$.

4. Experimental results

4.1. Mechanical behaviour law

We define the algebrical value F_g as the force induced by the generator on the cylinder, using the control system (cf. (*e*) in Fig. 2). This force, following the $\boldsymbol{z}_1$ direction and opposed to v_c velocity sense is equal to:

$$F_g = \frac{C_g}{r_p} = \pm \mathrm{k_p}\,|\,v_c\,|^{\mathrm{n_p}} \qquad (13)$$

where $\mathrm{k_p}$ is a proportional coefficient, $\mathrm{n_p}$ is an exponent and r_p is the radius of the pulley. The sign of F_g is always opposed to the sign of v_c.

When n_p = 1, k_p is simply a viscous damping coefficient. In this case, the force applied by the generator is directly proportional to the cylinder velocity. The n_p coefficient either allows to decrease or to increase continuously F_g for chosen speed ranges.

Fig. 5(a) shows the influence of n_p for a typical period of v_c. In the case of $n_p > 1$, the force is reduced for low-speed ranges ($v_c < 1\ \mathrm{m\ s^{-1}}$) whereas the force is amplified for high-speed ranges ($v_c > 1\ \mathrm{m\ s^{-1}}$). In the other case of $n_p < 1$ and tending to 0, F_g tends to a force opposed to the velocity and with a module equal to k_p.

To conserve cylinder oscillations due to the vortex locking on the cylinder, a limited displacement velocity range in which energy can be harvested without breaking this fluid structure interaction has to be set.

To do this, two ways are chosen. The first method consists in using a coefficient n_p greater than 1, as shown in Fig. 8. A simpler method consists of a binary approach, disconnecting the generator for speeds below a certain threshold as described below.

We define $H_r = [-v_{th}; +v_{th}]$ as the range of small cylinder velocities where the generator is disabled, with v_{th} being the velocity threshold value. F_g is also given by:

$$\begin{cases} F_g = \pm k_p \,|\, v_c \,|^{n_p} & \text{for} \quad v_c \notin [-v_{th}; +v_{th}] \\ F_g = 0 & \text{for} \quad v_c \in \,]-v_{th}; +v_{th}[\end{cases} \qquad (14)$$

Fig. 5(b) shows the periodic evolution of the cylinder displacement velocity along with the force induced by the generator. For example, the non harvesting velocity range H_r is clearly visible between 0.2 and 0.3 s.

Figure 5: Effect of n_p and v_{th} parameters on the force induced by the generator on the cylinder.

Then the mean power recovered by the generator $\overline{\mathcal{P}_g}$, being the temporal average of instantaneous power $\mathcal{P}_g$ on the duration of the test t_e can be written :

$$\overline{\mathcal{P}_g} = \frac{1}{t_e}\int_0^{t_e} \mathcal{P}_g \mathrm{d}t = \frac{1}{t_e}\int_0^{t_e} F_g v_c \mathrm{d}t \qquad (15)$$

The instantaneous hydraulic power $\mathcal{P}_f$ is obtained by integrating the kinetic energy of flow in time. The mean power $\overline{\mathcal{P}_f}$ stems from temporal average of instantaneous power $\mathcal{P}_f$ averaged on test duration t_e:

$$\overline{\mathcal{P}_f} = \frac{1}{t_e}\int_0^{t_e} \mathcal{P}_f \mathrm{d}t = \frac{1}{t_e}\int_0^{t_e} \frac{1}{2}\rho_f S u^3 \mathrm{d}t \qquad (16)$$

where ρ_f is the fluid density, *S* is the cross-sectional flow area covered by cylinder maximal displacement plus its diameter *D* multiplied by the cylinder length *L* (cf. Fig. 4). S is orthogonal to the fluid velocity *u* in the $\boldsymbol{x}_1$ direction.

$$S = (A + D)L \qquad (17)$$

Upstream kinetic energy is not significantly modified by energy harvesting. Indeed, for a fixed Q_v imposed by the pump, the wetted area in the channel is not modified by energy harvesting, which promotes for a constant kinetic energy. Finally the power coefficient, or efficiency, is defined as:

$$\eta = \overline{\mathcal{P}_g} / \overline{\mathcal{P}_f} \qquad (18)$$

Due to the confined aspect of the experimental setup, *u* is significantly increased near the cylinder because of the hydraulic section reduction. To compare hydropower harvesting performances with other works (Bernitsas et al. (2008) and Zhang et al. (2016)) the common definition of power coefficient for hydrokinetic turbines will be kept. This common definition as exposed above involves the instantaneous hydraulic power of the flow $\mathcal{P}_f$, usually calculated on cylinder effective surface (*L*

$\times D$) which increases η. However, it is deliberatly calculated here on the surface covered by cylinder displacement as it is commonly done for assessing harvestable energy by other hydroturbines types.

If the definition of the power coefficient is the same, it will be possible to compare the actual impact of confinement on efficiency with hydrokinetic turbines used in open environments.

4.2. Power coefficient, amplitude and mechanical frequency measurements

In what follows, we will study the impact of the four parameters k_p, n_p, m^* and v_{th} on power coefficient η, on amplitude A and on oscillation frequency. Experimental conditions are summarized in Table 1. Note that all experiments reported here were performed for the same inflow conditions, $u = 0.55\ m\ s^{-}1$. To observe the impact on A, we define the dimensionless parameter A/D.

A range of values for each parameter k_p, n_p, m^* and v_{th} is tested to assess their influence on power coefficient η, amplitude A and on oscillation frequency. The results are reported in Fig. 6(a) and 6(b). The influence of k_p on the system performances for different values of v_{th} and m^* is described in Fig. 6(b). We note that there is one optimal value of k_p for each value of v_{th} and m^*. Fig. 6(b) shows that if k_p is too low, around 13 here, the amplitude A is high as the vertical velocity. Consequently, a loss of energy is caused by viscous frictions. On the contrary, Fig. 6(b) also shows that for increasing values of k_p hence $|F_g|$, the normalized amplitude of cylinder A/D displacement decreases, and less energy is recovered by the system. Fig. 6(a) shows the evolution of efficiency in function of k_p and a maximum is clearly evidenced for each configuration. Note that when m^* ranges from 1.22 to 1.64, maximal efficiency η decreases by 10%. On the contrary, increasing the value of the velocity threshold increases η for this experimental setup Fig. 6(a).

Figure 6: Effect of v_{th} and m^* on amplitude and efficiency for different values of k_p.

Fig. 7 shows the influence of the generator force exponent n_p on the system behaviour, at fixed k_p = 16.

We see that η increases from 15 to 18 % for $1.1 \leq n_p \leq 1.3$. It also increases the oscillation amplitude.

Note that using Zhang et al. (2016) efficiency definition (calculated on cylinder surface), the power coefficient reaches a value of 43.7%, instead of 19%. Zhang et al. (2016) results show a maximum efficiency of 40.4% with an equilateral triangle prism.

Finally, Fig. 8 shows the influence of the different parameters on the oscillation frequency, $f_{c,e}$. This frequency increases while the breaking force F_g decreases, and declines slowly while the breaking force, F_g, becomes too high.

Figure 7: Amplitude and η in function of generator force exponent n_p for k_p = 16.

Figure 8: Frequency $f_{c,e} vs.\ k_p$ for different v_{th} and m^*.

4.3. Velocity field measurements with cylinder at rest

Fig. 9(b), 9(d), 9(f) and 9(h) show the spectrum of vertical velocity obtained at different lateral positions. At channel centerline (y = 30 cm) and at 18.5 cm from the wall (Fig. 9(b) and 9(d)), the spectrum is monomodal with a sharp peak centered at 1.3 Hz with a bandwidth of about 0.1 Hz. This frequency must correspond to vortex shedding frequency.

Davis et al. (1984) have shown an increase of shedding frequency in the case of confined flows around cylinders, which exceeds the Strouhal frequency. The experimental measurements (Fig. 9(b)) confirm this trend. Indeed, the shedding frequency without confinement should be equal to 0.91 Hz. But the measured frequency reaches the value of 1.31 Hz. This value corresponds to the Strouhal frequency obtained by taking into account the section reduction leading to velocity increase.

At 9.5 cm from the wall, the peak is still visible but its amplitude has decreased by more than 60 percent. Closer from the wall at 3.25 cm it has totally disappeared. In this last case the spectrum is quite similar to the spectrum without any cylinder. Another characteristic feature of the spectrum in the center region of the cylinder consists of an increase in velocity fluctuations, even at frequencies lower than peak frequency.

Figure 9: Vertical profile of horizontal mean velocity and spectrum of vertical velocity for cylinder at rest for different lateral positions (*y*). Red zone corresponds to the measurement of uncertainty in the x_1 direction.

Large differences in the vertical profiles of horizontal time averaged velocities were also observed in function of the lateral position (cf. Fig. 9(a), 9(c), 9(e), 9(g)). The fluid flows preferentially on the edges of the cylinder, where velocity fluctuations are low. The horizontal velocity is much lower in the central region whatever the depth, while large velocity fluctuations were observed. We can conclude that there are no vortices on a length approximately equal to one diameter on the edge of the cylinder, thereby reducing the useful length of the cylinder. Moreover a fully 3D flow develops away from the center of the cylinder due to significant edge effects. This phenomenom is even more significant as the aspect ratio is low.

As seen before the flow rate in the cylinder central region is lower than the flow rate averaged over the whole wetted section. Since vortex shedding frequency is a function of fluid velocity, low frequency fluctuations of horizontal velocity in the central region could explain the enlargement of vortex shedding frequency peaks. In order to monitor such a correlation, velocity signal of transducer, T_2, was analyzed in the following way:

• slipping Fast Fourrier Transform (FFT) of the velocity record is computed over a period of time corresponding to about 10 periods of average vortex shedding frequency and instantaneous main fluctuation frequency is determined.

• over the same period of time we compute the vertical profiles of average and fluctuant components of u_{T_2} velocity. Average vertical velocity at channel centerline being close to zero, the average component of velocity, u_{T_2}, is merely the projection of horizontal velocity while fluctuant component results mainly from vertical velocity fluctuation due to the low beam angle. Mean values over each velocity vertical profiles are afterwards computed.

An example of such data analysis is presented in Fig. 11. As seen, the peak frequency does not vary in a continuous way but presents rather sudden jumps. Although at times, average velocity and vortex shedding frequency show similar evolution as the average and fluctuant components of velocity do, no clear and systematic correlations between those flow parameters were observed. Due to the 3D character of the flow, a measurement of the third component of velocity is probably required for a better understanding of the flow phenomena.

4.4. Velocity field with cylinder in motion

All the results presented in what follows have been found with fixed parameters $k_{eq} = 830\ \mathrm{N\ m^{-1}}$, $n_p = 1$ and $k_p = 25\ \mathrm{N\ m^{-1}\ s^{-1}}$. Cylinder oscillations frequency always remained close to the natural vortex shedding frequency for a cylinder at rest with a lightly higher value . Instantaneous oscillations frequency evaluated as described formerly, also exhibits sudden jumps but remained stable for a much longer period of time (cf. Fig. 11). Note that those jumps do not influence average power.

Fluid velocity fluctuations peak frequency is always identical to cylinder one regardless of the lateral position. In Fig. 12(a), fluid spectrum was always computed at times when the cylinder oscillation frequency was close to 1.25 Hz. The difference with the cylinder at rest condition is that a peak is present even at the position closest to the wall, although with lower amplitude than in the central region. This difference probably arises from fluid motion generated by the cylinder oscillation. In the central region we observed a narrower peak, when compared to cylinder at rest, but of comparable amplitude which means that the total peak energy is lower despite the cylinder oscillations.

Figure 10: Evolution of peak frequency, mean and fluctuating components of u_{T_2} velocity as a function of time y = 0.31 m.

Figure 11: Evolution of cylinder and flow peak frequency and relative power as a function of time y = 0.31 m.

In what concerns horizontal velocity profiles (cf. Fig. 12(b)) the general features are the same as for cylinder at rest conditions. Profiles are flattened due to cylinder wake vertical periodical displacement.

Figure 12: Velocity measurements for oscillating cylinder.

5. Conclusion

This paper exposes experimental investigations of a stream generator based on vortex-induced vibrations phenomenon. A one degree of freedom immersed cylinder was tested in a confined situation. In this particular case, this signifies that aspect ratio is low and blockage ratio is large. An original way of optimization and some observations about the flow that can be drawn from this review are listed here.

First the experiments show that an optimization way can be found considering the control laws implemented in the generator control loops. Linear and non-linear laws were used : we show a strong influence of three parameters on the efficiency, the damping defined by both linear and exponential parameters and a velocity threshold .

Secondly ultrasonic profilers were used to obtain instantaneous velocity, average velocity fields and characteristic frequency. That was a good way to obtain essential information to comprehend the behaviour of the flow. Due to the confinement of the situation, the measured Strouhal frequency is 30% higher than expected by experimental parameters setup. Based on Eq. 1, we underline the effect of high blockage ratio on the flow. –Despite high blockage and low aspect ratio, we only observe a good fluid structure interaction around the middle of the cylinder.

Third, in the case of high blockage and low aspect ratio, the flow structure develops in the three dimensions of space, except for the center of the cylinder where the flow approaches a 2D pattern. Therefore, under such hydraulic and geometric conditions, a 3D numerical approach is essential to the modeling of this dynamic system formed by the confined flow and the oscillating cylinder. This numerical model can be used in the context of parametric optimization, but could also be used in the case of topological optimizations of the shape of the cylinder. Indeed, Zhang et al. (2016) have shown that for another range of mass coefficient and aspect ratio the shape itself of the immersed object could improve the efficiency of the system. This study reinforces the idea that an algorithm allowing the tracking of an optimal set of parameters in a multi-parameters space is a good way to improve efficiency.

Finally, this study was focused on optimizing the hydraulic efficiency of the system. Studies are currently being carried out on two aspects:

• The first concerning the optimization of the product-process-material trio in view of cost reduction.

• The second concerning the optimization of the energy transformation chain in its entirety and in particular the electro-mechanical conversion as well as its network coupling.

This will allow to estimate the cost per kWh.

6. Acknowledgement

The authors gratefully acknowledge ICube laboratory and the INSA of Strasbourg for making the two free-surface water channels available for the experiments and for supporting the developement of the renewelable energy branch of ICube.

Notation

A	=	mean amplitude of the cylinder oscillations (m)
C_a	=	added mass coefficient (–)
C_g	=	generator torque (N m)
C_{system}	=	damping coefficient (N m^{-1} s^{-1})
η	=	power coefficient or efficiency (–)
D	=	cylinder diameter (m)
$d_{1\%}$	=	first overshoot of the asymptotic value of static position (–)
F	=	external force (N)
$f_{c,e}$	=	cylinder oscillations main frequency in water (Hz)
$f_{o,e}$	=	body's natural frequency (Hz)
F_g	=	force induced by generator on cylinder (N)
F_b	=	breaking force (N)
f_s	=	Strouhal frequency (Hz)
f_v	=	vortex shedding frequency (Hz)
$f_{v,m}$	=	frequency of the periodic vortex mode (Hz)
h	=	water surface height (m)
I_g	=	generator intensity (A)
KC	=	Keulegan - Carpenter coefficient (–)
k_{eq}	=	system equivalent stiffness (N m^{-1})
k_1	=	constant stiffness (N m^{-1})
k_p	=	proportional coefficient for F_g calculation (–)
k_v	=	variable stiffness (N m^{-1})
l	=	channel width (m)
L	=	cylinder length (m)
m^*	=	mass ratio (–)
m_{eq}	=	system equivalent mass in vertical translation (kg)

m_a	=	added mass (kg)
$\mathrm{n_p}$	=	exponent coefficient for F_g calculation (–)
$\mathcal{P}_f$	=	instantaneous hydraulic power (W)
$\overline{\mathcal{P}_f}$	=	mean hydraulic power (W)
$\mathcal{P}_g$	=	instantaneous power recovered by the generator (W)
$\overline{\mathcal{P}_g}$	=	mean power recovered by the generator (W)
Q_v	=	instantaneous flow rate ($\mathrm{m^3 s^{-1}}$)
r_p	=	radius of generator polley (m)
R	=	Reynolds number (–)
S	=	surface described by cylinder oscillations ($\mathrm{m^2}$)
St	=	Strouhal number (–)
u	=	instantaneous horizontal velocity ($\mathrm{m\ s^{-1}}$)
$\overline{u}$	=	time averaged horizontal velocity ($\mathrm{m\ s^{-1}}$)
$u_{\mathrm{T_1}}$	=	velocity component in $\mathrm{T_1}$ beam direction ($\mathrm{m\ s^{-1}}$)
$\overline{u_{\mathrm{T_1}}}$	=	time averaged velocity component in $\mathrm{T_1}$ beam direction ($\mathrm{m\ s^{-1}}$)
$u_{\mathrm{T_2}}$	=	velocity component in $\mathrm{T_2}$ beam direction ($\mathrm{m\ s^{-1}}$)
$\overline{u_{\mathrm{T_2}}}$	=	time averaged velocity component in $\mathrm{T_2}$ beam direction ($\mathrm{m\ s^{-1}}$)
v	=	instantaneous vertical velocity ($\mathrm{m\ s^{-1}}$)
$\overline{v}$	=	time averaged horizontal velocity ($\mathrm{m\ s^{-1}}$)
V_{cyl}	=	immerged cylinder volume ($\mathrm{m^3}$)
v_c	=	projection of the cylinder velocity on $\boldsymbol{z}_1$ ($\mathrm{m\ s^{-1}}$)
v_{th}	=	velocity threshold ($\mathrm{m\ s^{-1}}$)
x_T	=	distance between transducers and cylinder central axis (m)
y	=	measurement system lateral position (m)
z	=	cylinder position (m)
Γ	=	projection of the cylinder acceleration on $\boldsymbol{z}_1$ ($\mathrm{m\ s^{-2}}$)
θ	=	angle between $\mathrm{T_1}$ and $\mathrm{T_2}$ ($^{\mathrm{o}}$)

θ_g	=	generator rotor angular position (^{o})
ξ	=	dimensionless damping parameter (–)
ρ_f	=	fluid density (kg m^{-3})
Ω_g	=	generator velocity (rad s^{-1})

References

Bal, J.-L., Chabot, B., 2001. Les énergies renouvelables. État de l'art et perspectives de développement. Earth and planetary sciences (333), 827–834.

Bernitsas, M., Raghavan, K., Ben-Simon, Y., Garcia, E., september 2008. VIVACE (Vortex Induced Vibration Aquatic Clean Energy) : a new concept in generation of clean and renewable energy from fluid flow. Journal of Offshore Mechanics and Arctic Engineering 130.

Blevins, R. D., 2001. Flow-Induced Vibration. Krieger Pub Co, 2^{nd} edition.

Chang, C., Kumar, R. A., Bernitsas, M., 2011. VIV and galloping of single circular cylinder with surface roughness at $2.0\times10^4 \leq \mathrm{Re} \leq 1.2\times10^5$. Ocean Engineering 38, 1713–1732.

Davis, R. W., Moore, E. F., Purtell, L. P., Jan. 1984. A numerical-experimental study of confined flow around rectangular cylinders. Physic of Fluids 27 (1), 4659.

Ding, L., Bernitsas, M.-M., Kim, E. S., 2013. 2-d urans vs. experiments of flow induced motions of two circular cylinders in tandem with passive turbulence control for 30,000 $<$ re $<$ 105,000. Ocean Engineering 72.

Gaurier, B., Germain, G., Facq, J., Baudet, L., Birades, M., Schoefs, F., mars 2003. Marine growth effects on the hydrodynamical behaviour of circular structures.

Grouthier, C., Michelin, S., Bourguet, R., Modarres-Sadeghi, Y., Langre, E. D., 2014. On the efficiency of energy harvesting using vortex-induced vibrations of cables. Journal of Fluids and Structures 49.

Kiu, K., Stappenbelt, B., Thiagarajan, K., 2011. Effects of uniform surface roughness on vortex-induces vibration of towed vertical cylinders. Journal of Sound and Vibration 330, 4753–4763.

Lee, J., Bernitsas, M., 2011. High-damping, high-reynolds viv tests for energy harnessing using the vivace converter. Ocean Engineering 38, 1697–1712.

Lee, J., Xiros, N., Bernitsas, M., 2011. Virtual damper-spring system for viv experiments and hydrokinetic energy conversion. Ocean Engineering 38, 732–747.

Meliga, P., Chomaz, K.-M., Gallaire, F., Aot 2011. Utiliser les vibrations induites par vortex et la théorie du contrôle pour extraire de l'énergie d'un écoulement.

Pallares, A., François, P., Pons, M.-N., Schmitt, P., Jan. 2011. Suspended particles in wastewater: their optical, sedimentation and acoustical characterization and modeling. Water Science & Technology 63 (2).

Raghavan, K., Bernitsas, M., Apr. 2011. Experimental investigation of Reynolds number effect on vortex induced vibration of rigid circular cylinder on elastic supports. Ocean Engineering 38 (5-6), 719–731.

Rajaona, R., Groussard, F., Levenez, M., Lebey, M., Mar. 2003. Sur la visualisation de l'écoulement autour d'un cylindre oscillant au voisinage d'une surface libre. Poitiers.

Singh, K., Michelin, S., de Langre, E., 2012. Energy harvesting from axial fluid-elastic instabilities of a cylinder. Journal of Fluids and Structures 30, 159 – 172.

Zdravkovich, M.-M., 1997. Flow Around Circular Cylinders. Fundamentals. Vol. 1. Oxford University Press.

Zhang, J., Liu, F., Lian, J., Yan, X., Ren, Q., 2016. Flow induced vibration and energy extraction of an equilateral triangle prism at different system damping ratios. Energies 938 (9).

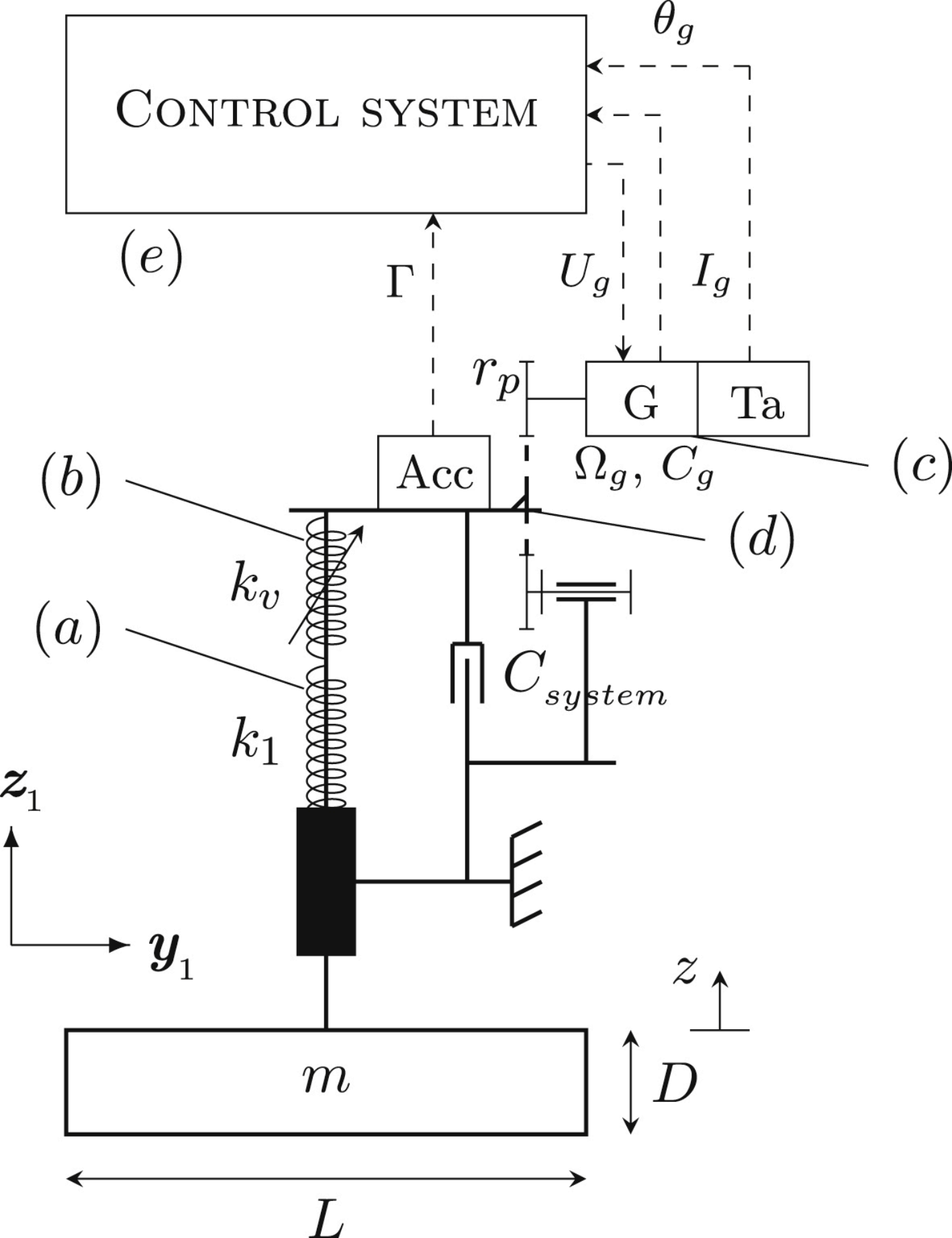
Control system
θ_g
(e)
Γ
U_g
I_g
r_p
G
Ta
Acc
Ω_g, C_g
(b)
(c)
(d)
k_v
(a)
C_{system}
k_1
z_1
y_1
z
m
D
L

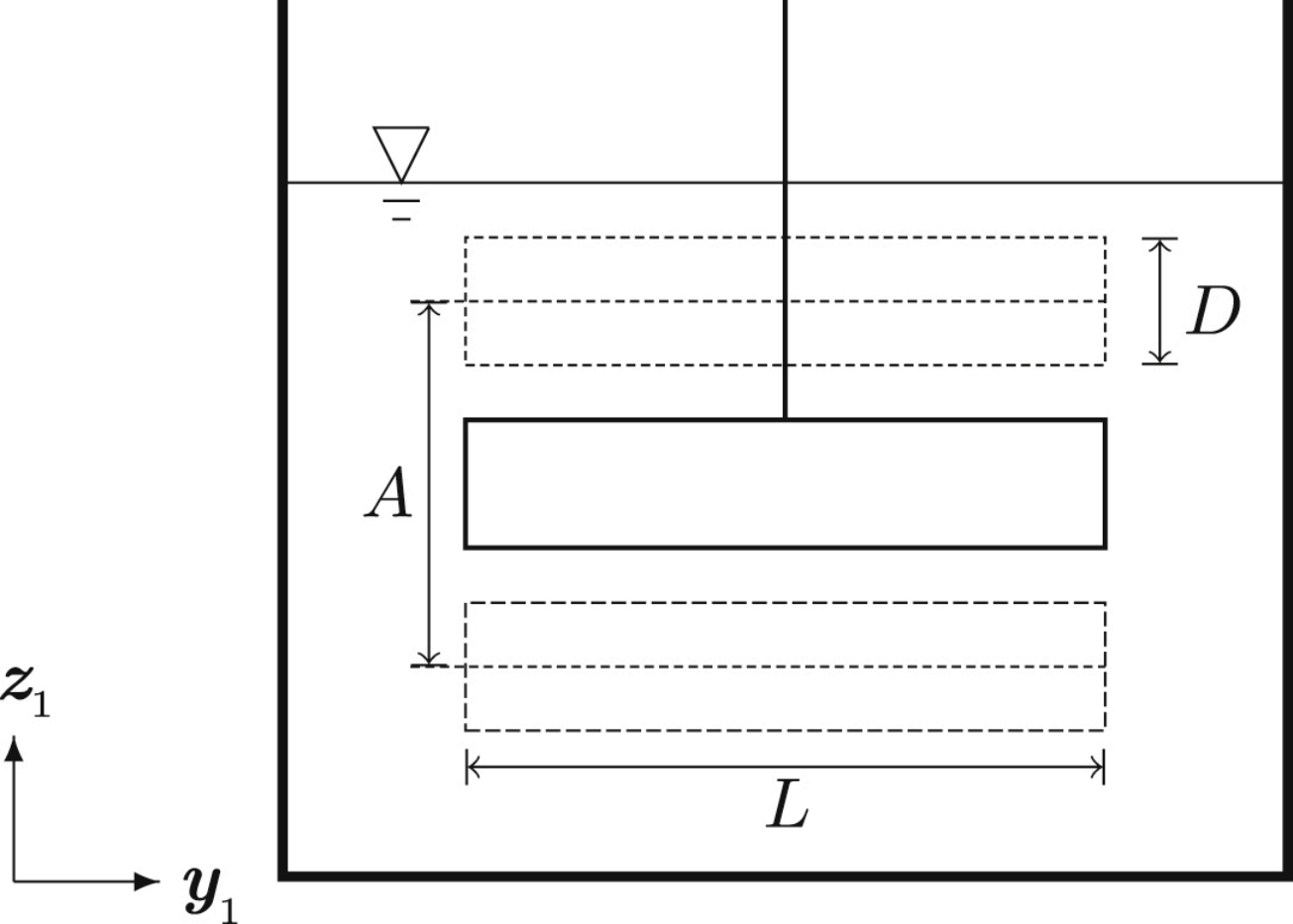
D
A
L
z_1
y_1

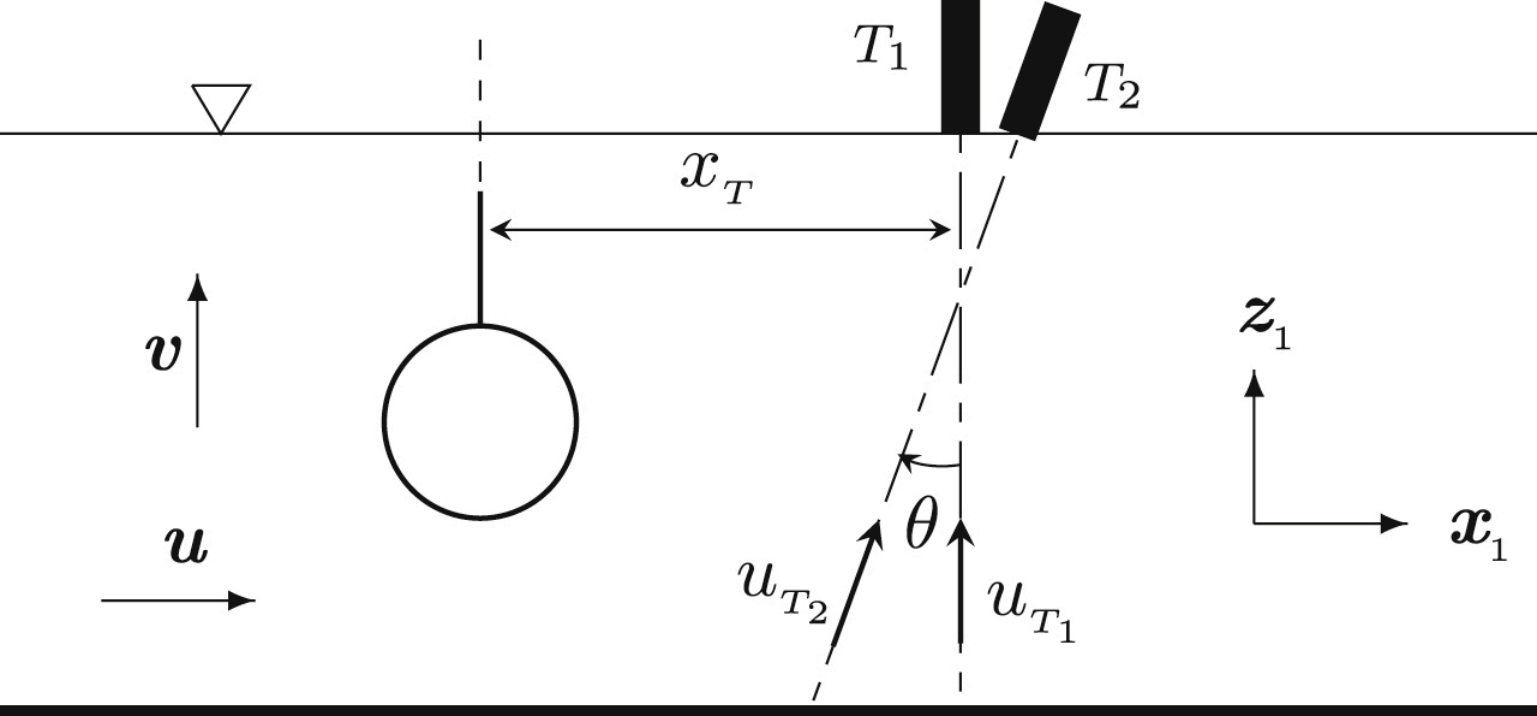
T_1
T_2
x_T
v
u
θ
u_{T_2}
u_{T_1}
z_1
x_1

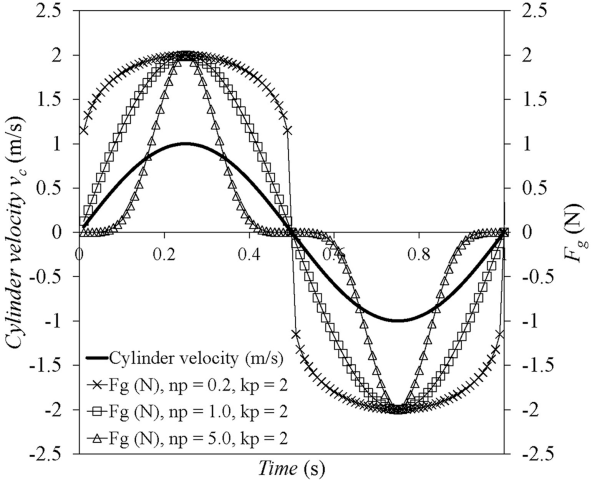

(a) Impact of n_p values on the temporal evolution of F_g for a typical period of v_c.

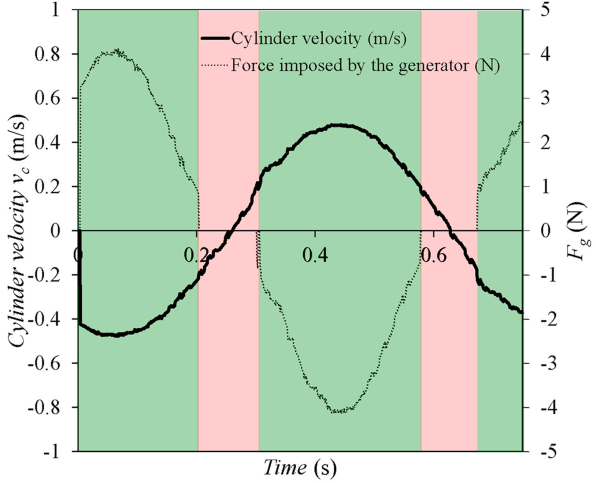

(b) Example of typical energy harvesting configuration with cylinder velocity and force induced by the generator represented along with the harvesting range H_r = [-0.2 ; +0.2. Velocity threshold being equal to 0.2 m/s. Green (resp. red) areas represent harvesting time periods (resp. non harvesting).

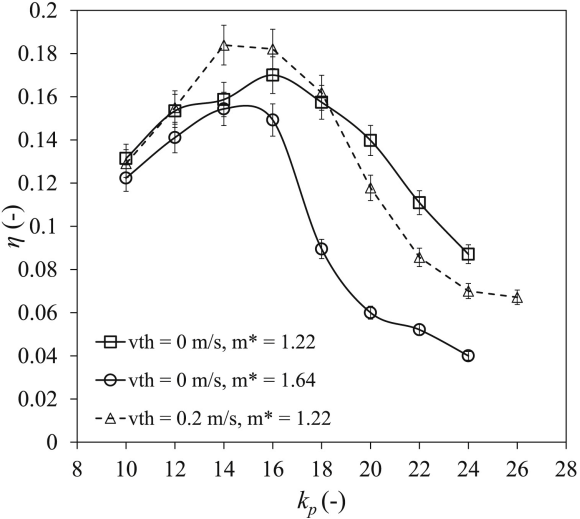

(a) Efficiency η *vs.* k_p for different v_{th} and m^* ($n_p = 1$).

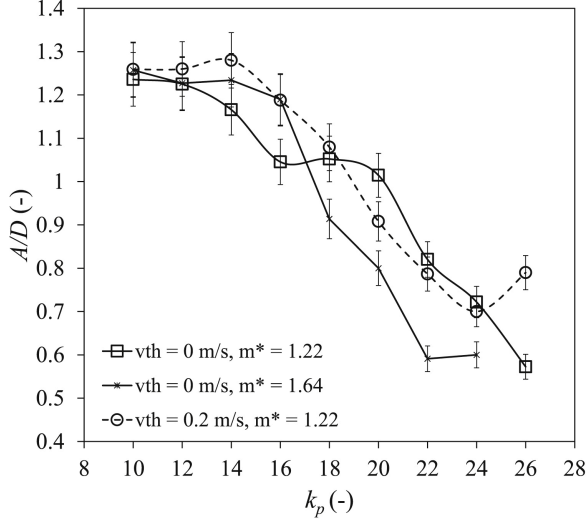

(b) Amplitude *vs.* k_p for different v_{th} and m^* ($n_p = 1$).

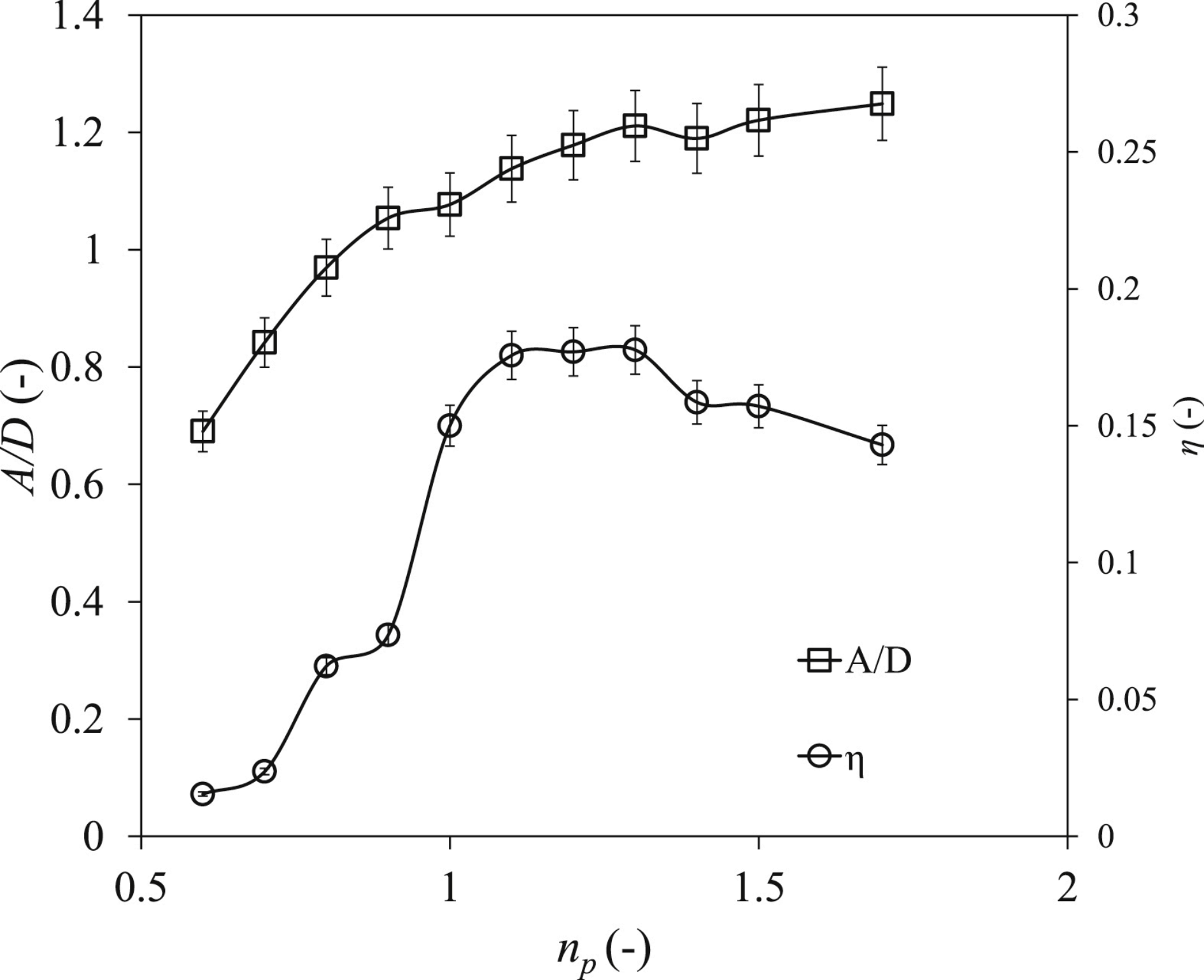
1.4
1.2
1
0.8
0.6
0.4
0.2
0
A/D (-)
0.3
0.25
0.2
0.15
0.1
0.05
0
η (-)
0.5
1
1.5
2
n_p (-)
A/D
η

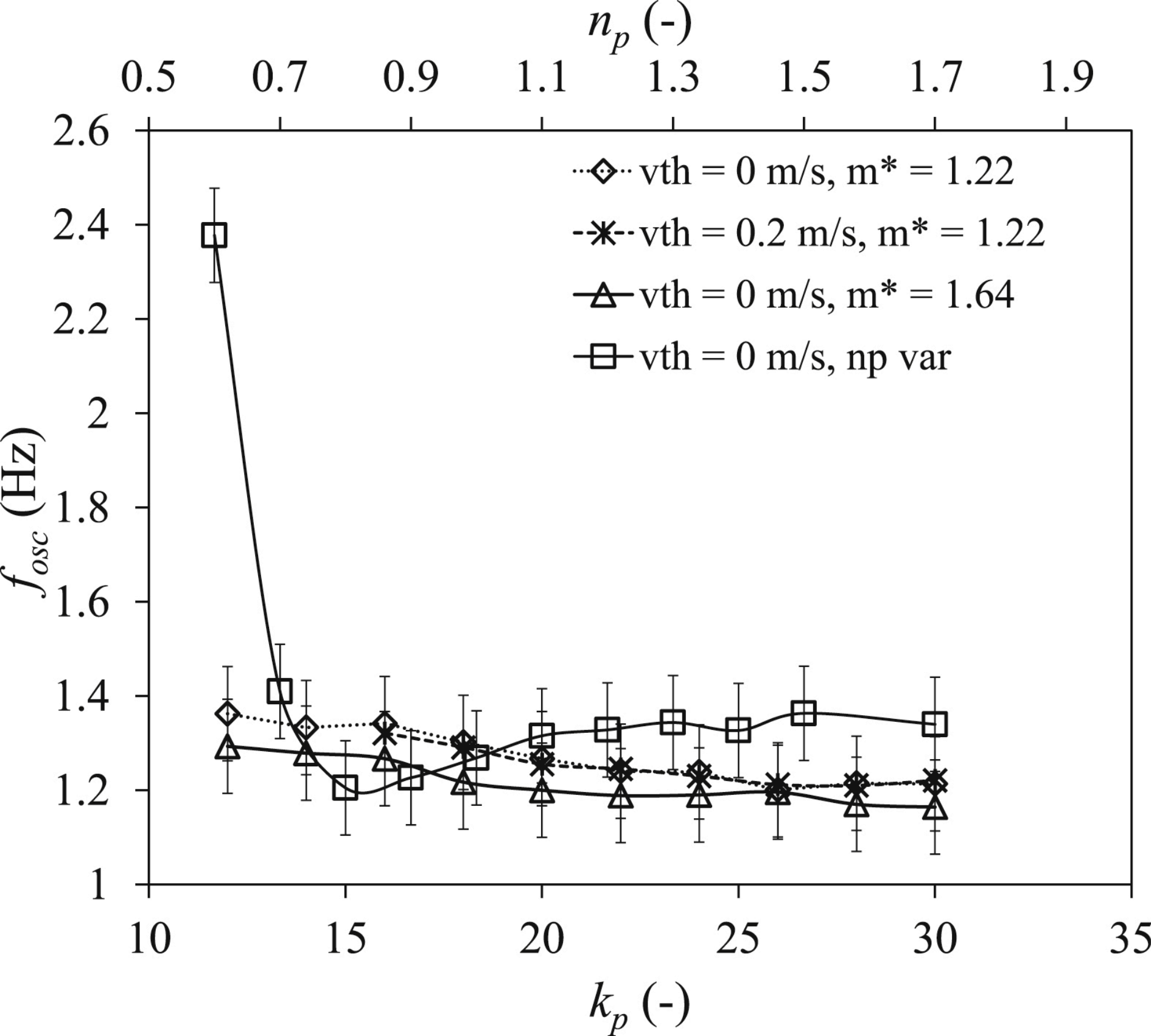
n_p (-)
0.5
0.7
0.9
1.1
1.3
1.5
1.7
1.9
2.6
2.4
2.2
2
1.8
1.6
1.4
1.2
1
f_{osc} (Hz)
vth = 0 m/s, m* = 1.22
vth = 0.2 m/s, m* = 1.22
vth = 0 m/s, m* = 1.64
vth = 0 m/s, np var
10
15
20
25
30
35
k_p (-)

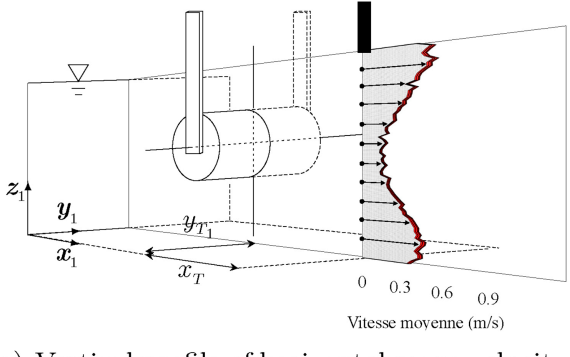

(a) Vertical profile of horizontal mean velocity at $y_1 = 30$ cm.

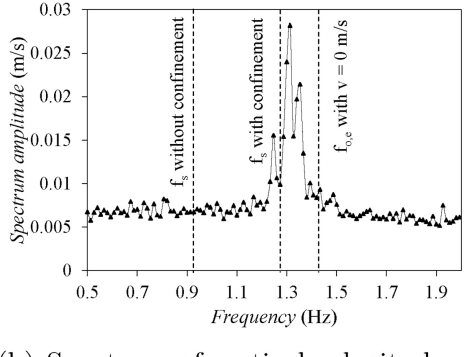

(b) Spectrum of vertical velocity behind the cylinder axis ($y_1 = 30$ cm).

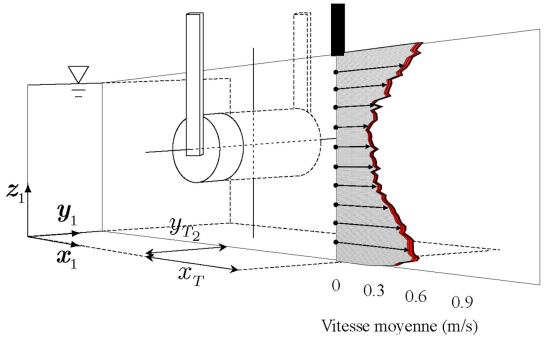

(c) Vertical profile of horizontal mean velocity at $y_1 = 18.5$ cm.

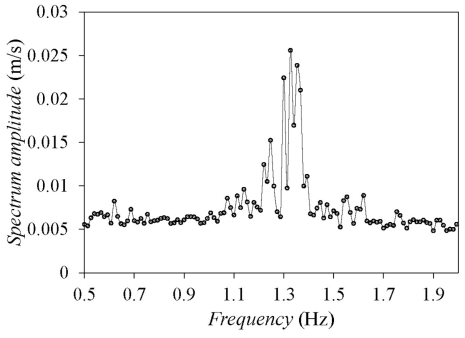

(d) Spectrum of vertical velocity behind the cylinder axis ($y_1 = 18.5$ cm).

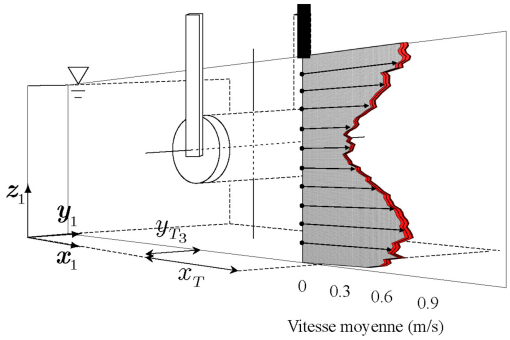

(e) Vertical profile of horizontal mean velocity at $y_1 = 9.5$ cm.

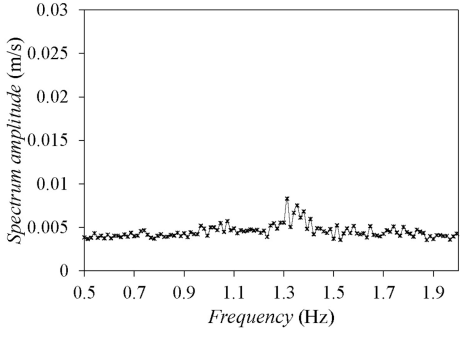

(f) Spectrum of vertical velocity behind the cylinder axis ($y_1 = 9.5$ cm).

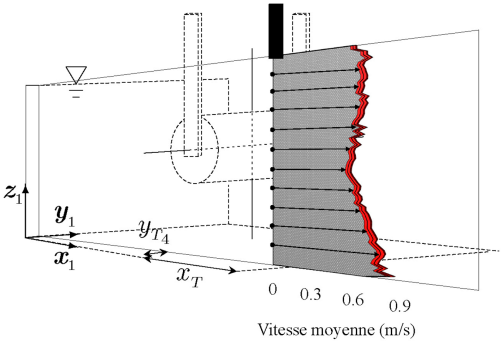

(g) Vertical profile of horizontal mean velocity at $y_1 = 3.25$ cm.

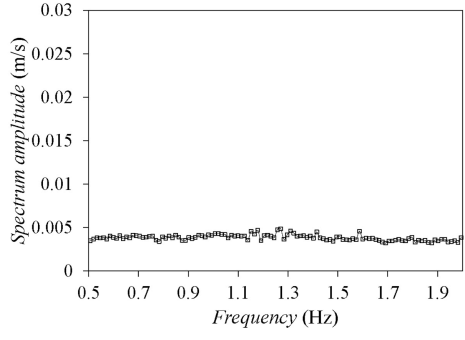

(h) Spectrum of vertical velocity behind the cylinder axis ($y_1 = 3.25$ cm).

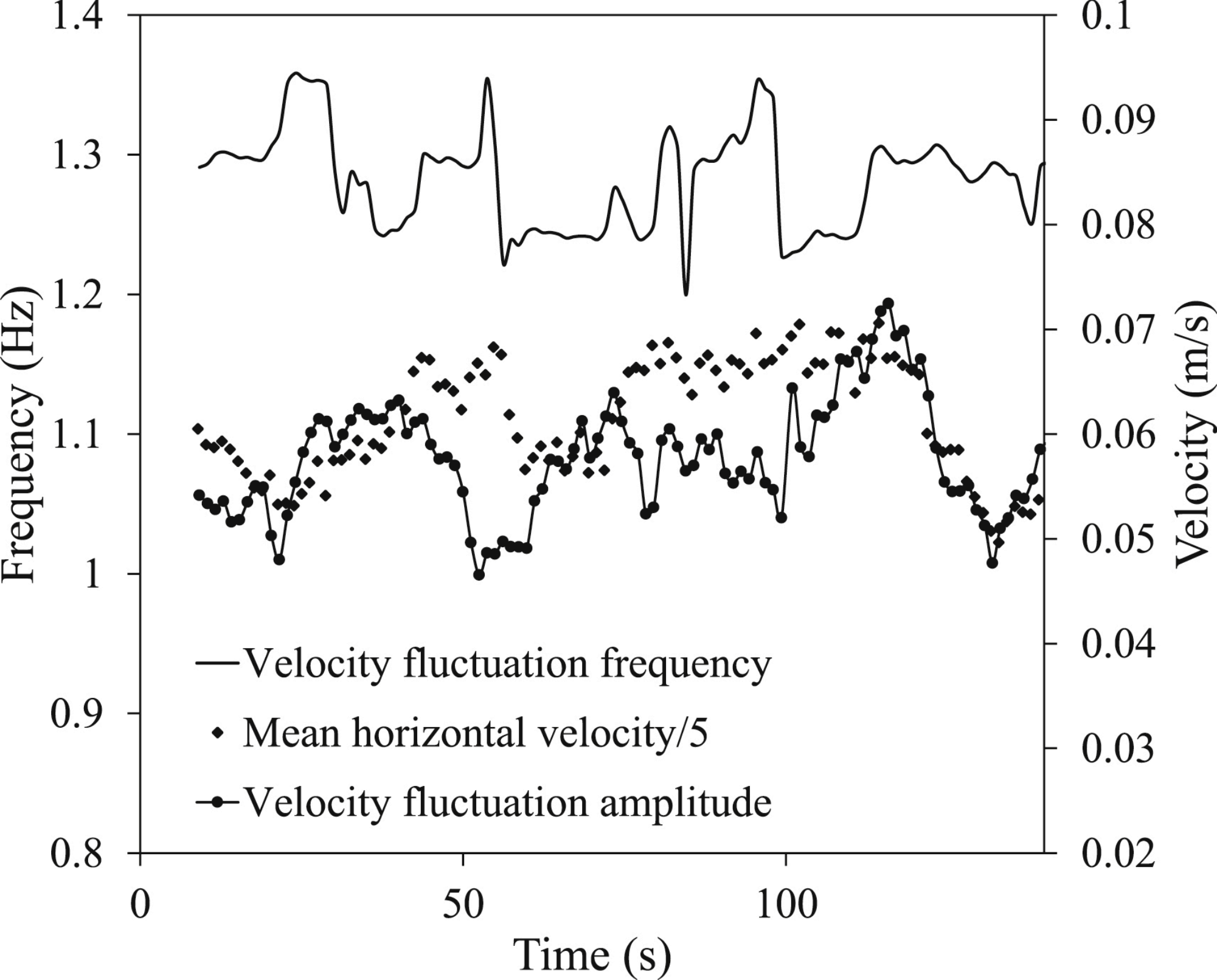
1.4
1.3
1.2
1.1
1
0.9
0.8
Frequency (Hz)
0.1
0.09
0.08
0.07
0.06
0.05
0.04
0.03
0.02
Velocity (m/s)
0
50
100
Time (s)
Velocity fluctuation frequency
Mean horizontal velocity/5
Velocity fluctuation amplitude

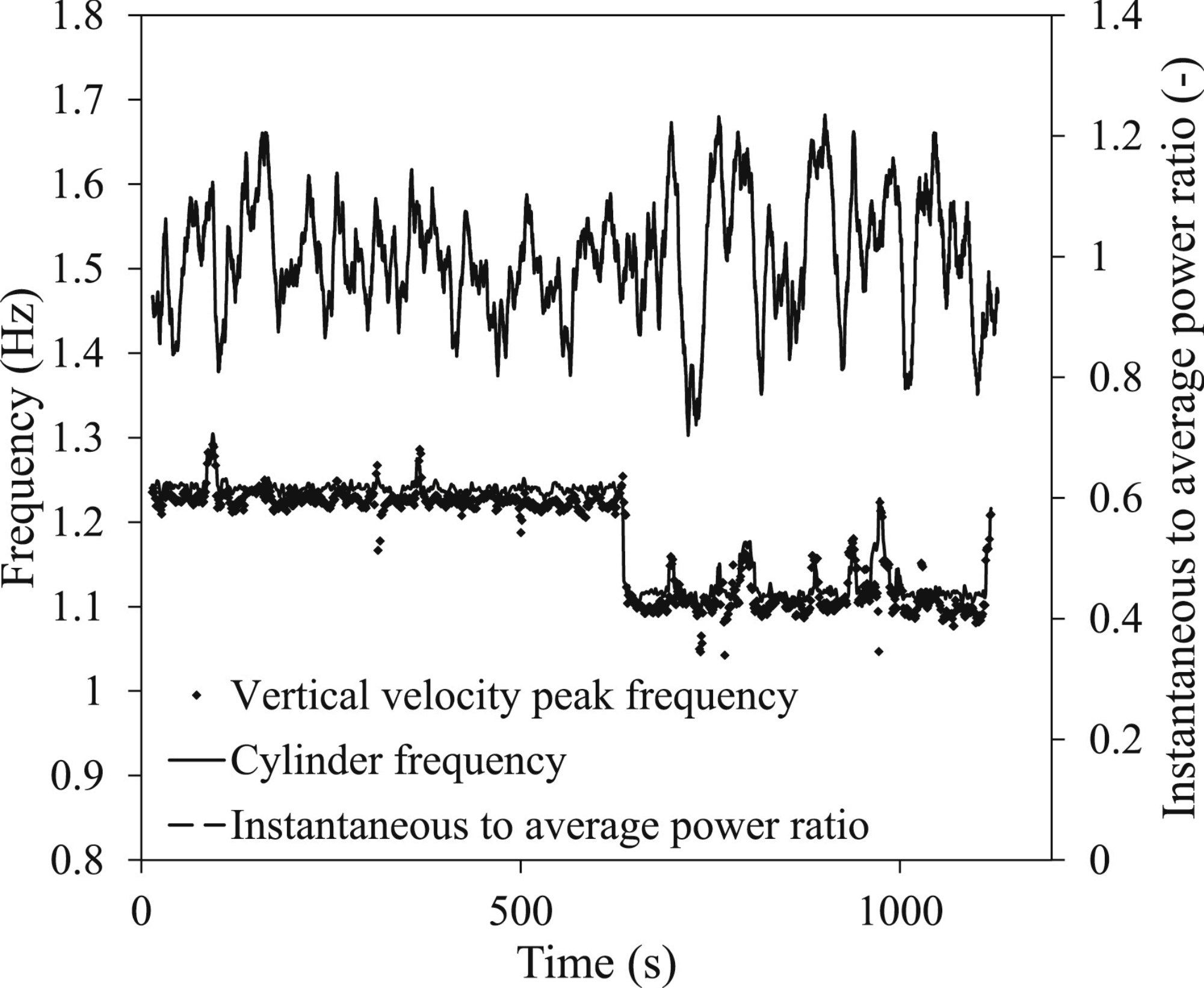
1.8
1.7
1.6
1.5
1.4
1.3
1.2
1.1
1
0.9
0.8
Frequency (Hz)
1.4
1.2
1
0.8
0.6
0.4
0.2
0
Instantaneous to average power ratio (-)
0
500
1000
Time (s)
Vertical velocity peak frequency
Cylinder frequency
Instantaneous to average power ratio

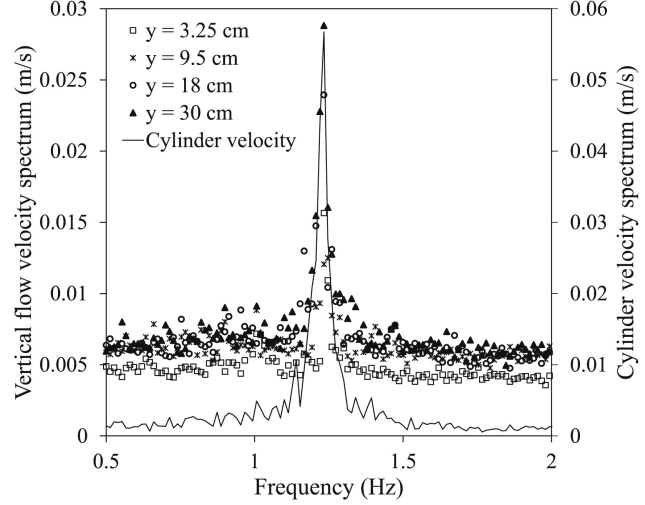

(a) Spectrum of vertical velocity at various lateral positions.

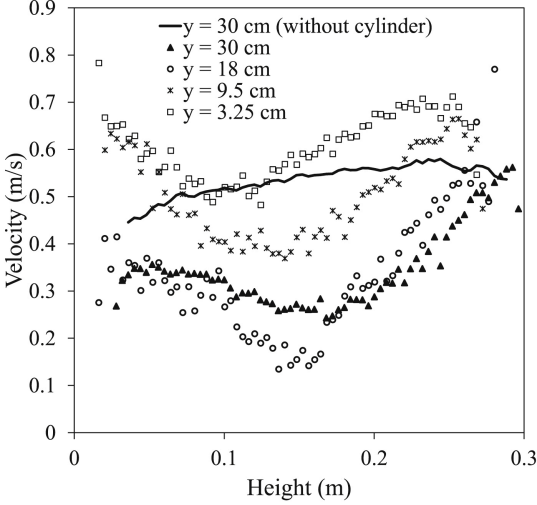

(b) Vertical profiles of horizontal average velocity at various lateral position.

Nicolas Dellinger
Icube Laboratory
2 rue Boussinguault
67000 Strasbourg – France
Nicolas.dellinger@unistra.fr
Phone: +33607115397
Fax: +33388144790

may 22th 2017

Renewable Energy

Subject: Submission of revised manuscript

Dear Editor,

You can find hear the highlights of the revised manuscript entitled "An experiment of a hydropower conversion system based on vortex-induced vibrations in a confined channel" submitted to the Renewable Energy journal.

- A hydro-power conversion system based on vortex-induced vibrations phenomenom is investigated experimentally

- We propose a study of the effects of a confined flow on the system efficiency

- We higlight feasible improvements, particularly through automatic control strategies

- We show strong influence of confinement on the flow topology through velocity field measurements using pulse-pair method

Sincerely,

Dellinger, Nicolas.